RSC Advances

PAPER

View Article Online
View Journal | View Issue

Cite this: *RSC Adv.*, 2022, **12**, 34962

Structurally diverse biflavonoids from *Dysosma versipellis* and their bioactivity†

Yan-Jun Sun, *[abc] Rui-Jie Han,[ab] Hong-Yun Bai,[ab] Hao-jie Wang,[ab] Meng Li,[ab] Ying-Ying Si,[ab] Jun-Min Wang,[ab] Jian-Hong Gong,[ab] Hui Chen[ab] and Wei-Sheng Feng *[ab]

Five pairs of new biflavonoid enantiomers, (±)-dysosmabiflavonoids A–E (**1–5**), two new biflavonoids, dysosmabiflavonoids F–G (**6–7**), and four biosynthetically related precursors (**8–11**) were isolated from the roots and rhizomes of *Dysosma versipellis*. Their structures were elucidated by extensive spectroscopic analysis, including HR-ESI-MS and 2D NMR. Their absolute configurations were determined by comparison of the calculated and experimental ECD spectra. All isolated compounds were evaluated for AChE inhibitory activity. Compounds **6** and **7** exhibited more potent inhibitory activities with IC_{50} values of 1.42 and 0.73 μM, respectively, than their biosynthetically related precursors kaempferol (**8**, 17.90 μM) and quercetin (**9**, 3.96 μM). The preliminary structure–activity relationship study indicated that the connection mode of biflavonoid subunits, oxidation degree of the C ring, and 3,4-dihydroxy group of the B ring were important structural factors for AChE inhibitory activity. Racemates **1–5** and their corresponding levorotatory and dextrorotatory enantiomers were tested for their potential to impede the generation of NO in lipopolysaccharide-stimulated RAW264.7 cells, and their mushroom tyrosinase inhibitory effect. Racemate **1** displayed more potent mushroom tyrosinase inhibitory activity (IC_{50}, 28.27 μM) than the positive control kojic acid (IC_{50}, 32.59 μM). *D. versipellis* may have therapeutic potential for melanogenesis disorders and neurodegenerative diseases.

Received 3rd November 2022
Accepted 29th November 2022

DOI: 10.1039/d2ra06961j

rsc.li/rsc-advances

Introduction

Neurodegenerative diseases are an internationally faced public health problem. Acetylcholinesterase (AChE) catalyzes the hydrolysis of the neurotransmitter acetylcholine, which plays a key role in memory and cognition.[1] It is also the key enzyme target for treatments of myasthenia gravis, glaucoma, Alzheimer's disease, Parkinson's disease, and other neurodegenerative diseases.[2] Although a few cholinesterase inhibitors from synthetic and natural origins are available in the drug market, they are used only for symptomatic treatment. Moreover, side effects and relatively low bioavailability limit their clinical applications.[3] There is still a great demand to discover new cholinesterase inhibitors, which can improve cholinergic transmission in neurodegenerative diseases. Traditional Chinese medicine has become a promising source of structurally novel cholinesterase inhibitors.

A perennial herb of the Berberidaceae family, *Dysosma versipellis* (Hance) M. Cheng ex Ying, is widely distributed in the central/south regions of China.[4] Its roots and rhizomes, called "Bajiaolian" in Chinese, have the functions of eliminating phlegm, detoxification, removing blood stasis and dispersing knots.[5] As a common folk medicine, it has a satisfactory effect on the treatment of parotitis,[4] cough, sore throat, scrofula, nameless swollen venom/carbuncles, snake bite, fall injury, rheumatoid arthritis,[5] epidemic encephalitis B, parasites, tumor,[6] lumbago, skelalgia,[7] ulcer,[8] weakness, condyloma accuminata, lymphadenopathy,[9] pyogenic infection,[10] hemiplegia, joint pain,[11] and syphilis[12] since the Han dynasty in China. Its previous phytochemical and pharmacological investigations revealed the presense of bioactive biflavonoids,[13–16] and their neuraminidase inhibitory[13] and cytotoxic properties.[14] In our search for bioactive natural products, five pairs of new biflavonoid enantiomers, (±)-dysosmabiflavonoids A–E (**1–5**), two new biflavonoids, dysosmabiflavonoids F–G (**6–7**), along with four biosynthetically related precursors (**8–11**) (Fig. 1) were isolated from the roots and rhizomes of *D. versipellis*. Reported herein are their isolation, structure elucidation, and bioactive evaluation.

[a]*Co-construction Collaborative Innovation Center for Chinese Medicine and Respiratory Diseases by Henan & Education Ministry of P. R. China, Henan University of Chinese Medicine, Zhengzhou 450046, P. R. China. E-mail: sunyanjunily@126.com; fwsh@hactcm.edu.cn*

[b]*School of Pharmacy, Henan University of Chinese Medicine, Zhengzhou 450046, P. R. China*

[c]*Henan Research Center for Special Processing Technology of Chinese Medicine, Zhengzhou, 450046, P. R. China*

† Electronic supplementary information (ESI) available: UV, IR, HR-ESI-MS, ECD, 1D and 2D NMR spectra for compounds **1–7**. See DOI: https://doi.org/10.1039/d2ra06961j

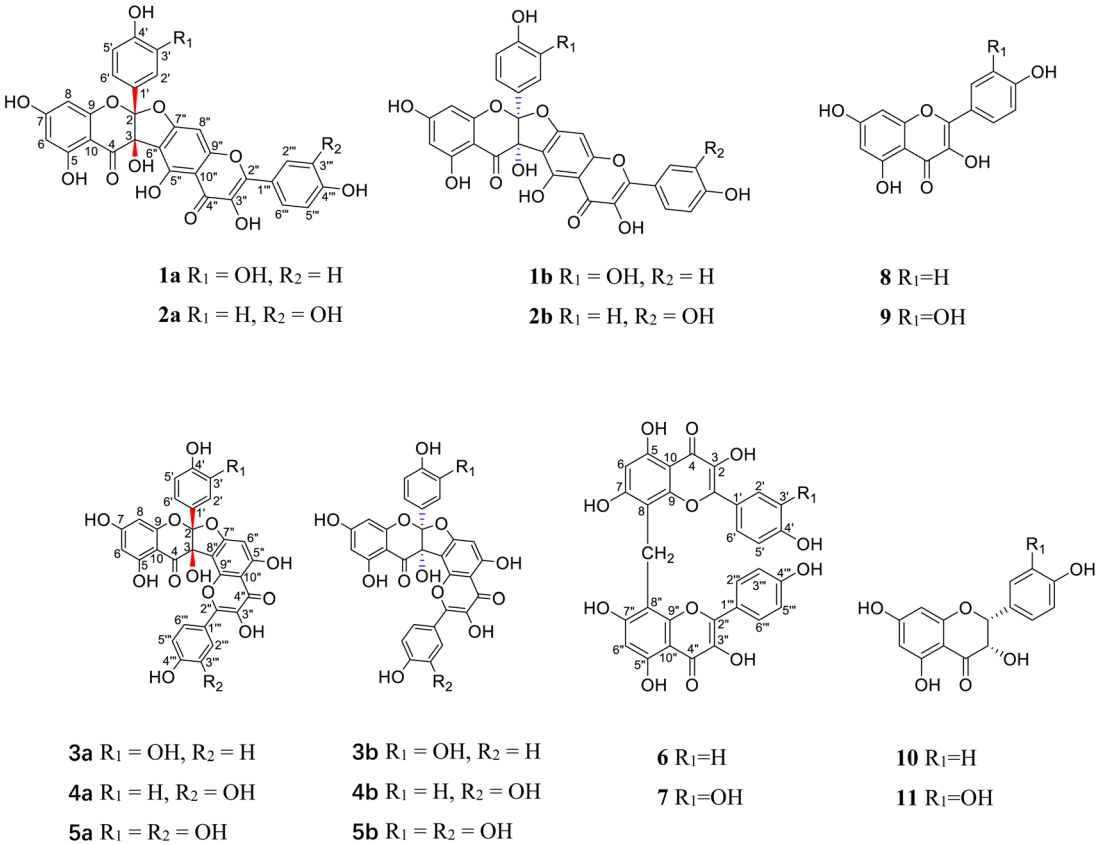

Fig. 1 The structures of compounds **1–11**.

Results and discussion

Compound **1** was obtained as a yellow amorphous powder and possessed a molecular formula $C_{30}H_{18}O_{13}$ with twenty-two degrees of unsaturation, as revealed from its HR-ESI-MS analysis (*m*/*z* 587.0806 $[M + H]^+$, calcd for $C_{30}H_{19}O_{13}$, 587.0826). The IR spectrum displayed two carbonyl groups (1726, 1635 cm^{-1}), hydroxy groups (3374 cm^{-1}), aromatic rings (1607, 1512 cm^{-1}) and tertiary alcohol (1179 cm^{-1}). The UV spectrum exhibited absorption maxima characteristic for flavonol at 275 and 360 nm. The ^{13}C NMR (Table 1) and HSQC spectra revealed one biflavone skeleton including two carbonyl groups δ_C 176.6, 190.1 (characteristic of a flavonol and a flavanonol, respectively), four benzene rings, two oxygen-bearing olefinic carbons δ_C 147.8, 136.1, two aliphatic quaternary carbons δ_C 117.6, 79.1. The ^1H NMR spectrum (Table 2) showed four sets of aromatic systems including one *para*-disubstituted benzene ring δ_H 8.08 (2H, d, J = 8.5 Hz), 6.94 (2H, d, J = 8.5 Hz), one penta-substituted benzene ring δ_H 7.01 (1H, s), one 1,3,4-tri-substituted benzene ring δ_H 6.89 (1H, s), 6.72 (1H, d, J = 8.6 Hz), 6.75 (1H, d, J = 8.6 Hz), and one 1,2,3,5-tetra-substituted benzene ring δ_H 5.86 (1H, s) and 5.78 (1H, s). The HMBC correlations (Fig. 2) of the aromatic protons δ_H 8.08 (2H, d, J = 8.5 Hz, H-2‴, 6‴) with C-2″ (δ_C 147.8), in combination with one penta-substituted benzene ring at δ_H 7.01 (1H, s), indicated that compound **1** contained kaempferol as a subunit.[17] Another subunit was identified as dihydroquercetin by the HMBC cross peak of the aromatic protons δ_H 6.89 (1H, s, H-2′) and 6.75 (1H, d, J = 8.6 Hz, H-6′) with C-2 (δ_C 117.6), one 1,2,3,5-tetra-substituted benzene ring δ_H 5.86 (1H, s), 5.78 (1H, s), and two aliphatic quaternary carbons δ_C 117.6, 79.1. A careful comparison of the ^{13}C NMR spectra of **1** with kaempferol indicated that the subunit of kaempferol was substituted at C-6 and C-7, which was confirmed by the chemical shift change from δ_C 156.8 (C-5′), 110.3 (C-6″), 164.3 (C-7″), 91.1 (C-8″), and δ_H 7.01 (1H, s, H-8″) in **1** to δ_C 160.7 (C-5), 98.2 (C-6), 163.9 (C-7), 93.5 (C-8), and δ_H 6.48 (1H, d, J = 2.0 Hz, H-8) in kaempferol.[17] An ether bridge C-2-O-C-7″ and a C-3-C-6″ bond between the two flavonoid subunits were determined by two aliphatic quaternary carbons [one di-oxygenated δ_C 117.6 (C-2), one mono-oxygenated δ_C 79.1 (C-3)].[18] The planar structure of **1** (Fig. 1) was determined by detailed elucidation on 1D and 2D NMR data. Despite repeated experiments, suitable single crystals of **1** for X-ray diffraction were not obtained successfully. NOESY experiments failed to provide any correlations between the two flavonoid subunits. Compound **1** showed no distinct Cotton effects (200–400 nm) at all examined concentrations, indicating it was a racemic mixture. This result is also consistent with the observation that **1** was optically inactive. Racemate **1** was resolved into **1a** and **1b** in a ratio of approximately 1 : 1 by a chiral Daicel PAK AD-H column. As expected, the ECD spectra of **1a** and **1b** showed opposite Cotton effects. The absolute configurations of C-2 and C-3 were extrapolated by comparing the experimental with calculated ECD spectra, the latter performed by density

Table 1 ^{13}C NMR data (125 MHz) of **1–7** in DMSO-d_6 (δ in ppm)

No.	1	2	3	4	5	6	7
2	117.6 C	117.8 C	117.8 C	117.7 C	117.8 C	146.9 C	146.7 C
3	79.1 C	79.2 C	79.9 C	79.9 C	79.9 C	135.4 C	135.4 C
4	190.1 C	190.7 C	191.0 C	190.5 C	191.0 C	176.2 C	176.1 C
5	163.3 C	163.4 C	163.5 C	163.5 C	163.5 C	158.4 C	158.4 C
6	97.5 CH	96.9 CH	97.0 CH	97.1 CH	97.0 CH	97.9 CH	98.0 CH
7	168.9 C	167.8 C	167.9 C	168.1 C	167.9 C	162.1 C	162.1 C
8	95.4 CH	95.1 CH	95.3 CH	95.3 CH	95.3 CH	104.6 C	104.7 C
9	160.4 C	160.4 C	160.6 C	160.3 C	160.6 C	153.8 C	153.8 C
10	97.8 C	98.4 C	98.6 C	98.3 C	98.6 C	102.8 C	102.6 C
1′	123.9 C	123.7 C	123.7 C	123.4 C	123.7 C	122.1 C	122.5 C
2′	114.5 CH	128.8 CH	114.5 CH	128.3 CH	114.5 CH	129.6 CH	115.2 CH
3′	144.6 C	115.2 CH	144.7 C	114.8 CH	144.7 C	115.4 CH	145.0 C
4′	146.8 C	159.1 C	146.9 C	158.7 C	146.9 C	159.1 C	147.6 C
5′	114.9 CH	115.2 CH	115.5 CH	114.8 CH	115.1 CH	115.4 CH	115.6 CH
6′	118.1 CH	128.8 CH	118.2 CH	128.3 CH	118.2 CH	129.6 CH	120.0 CH
2″	147.8 C	148.0 C	147.5 C	147.5 C	147.5 C	146.9 C	146.6 C
3″	136.1 C	136.2 C	136.1 C	136.0 C	136.1 C	135.4 C	135.3 C
4″	176.6 C	176.6 C	176.3 C	176.2 C	176.2 C	176.2 C	176.1 C
5″	156.8 C	156.9 C	163.9 C	163.8 C	163.8 C	158.4 C	158.3 C
6″	110.3 C	110.0 C	94.8 CH	94.7 CH	94.7 CH	97.9 CH	97.9 CH
7″	164.3 C	164.3 C	164.9 C	164.8 C	164.8 C	162.1 C	162.1 C
8″	91.1 CH	91.1 CH	106.3 C	106.1 C	106.1 C	104.6 C	104.6 C
9″	157.2 C	157.2 C	151.2 C	151.5 C	151.2 C	153.8 C	153.7 C
10″	105.6 C	105.7 C	105.2 C	105.2 C	105.2 C	102.8 C	102.6 C
1‴	121.3 C	121.6 C	121.4 C	121.7 C	121.7 C	122.1 C	122.1 C
2‴	129.7 CH	115.3 CH	130.2 CH	116.6 CH	116.2 CH	129.6 CH	129.5 CH
3‴	115.5 CH	145.2 C	115.3 CH	145.4 C	144.9 C	115.4 CH	115.4 CH
4‴	159.6 C	148.2 C	159.6 C	148.1 C	148.1 C	159.1 C	159.0 C
5‴	115.5 CH	115.7 CH	115.3 CH	115.3 CH	115.3 CH	115.4 CH	115.4 CH
6‴	129.7 CH	120.2 CH	130.2 CH	120.5 CH	120.5 CH	129.6 CH	129.5 CH
8-CH_2-8″						16.4 CH_2	16.5 CH_2

functional theory. A comparison of the observed ECD spectra for **1a** and **1b** with the calculated ECD spectra for the (2*S*, 3*S*)-**1** and (2*R*, 3*R*)-**1** is shown in Fig. 3. The overall ECD spectra for (2*S*, 3*S*)-**1** and (2*R*, 3*R*)-**1** are in good accordance with the experimental ECD for **1a** and **1b**, respectively. Therefore, the absolute configurations of **1a** and **1b** were respectively deduced to be 2*S*, 3*S* and 2*R*, 3*R*. Thus, compounds **1a** and **1b** were determined as (2*S*,3*S*)-3,5,7,3′,4′-pentahydroxyflavanone-(2-O-7″:3-6″)-3″,5″,4‴-trihydroxyflavone and (2*R*,3*R*)-3,5,7,3′,4′-pentahydroxyflavanone-(2-O-7″:3-6″)-3″,5″,4‴-trihydroxyflavone, and named as (+)-dysosmabiflavonoid A and (−)-dysosmabiflavonoid A, respectively.

Compound **2** was obtained as a yellow amorphous powder. It gave the same molecular formula $C_{30}H_{18}O_{13}$ as that of **1**, based

Table 2 ^{1}H NMR data (500 MHz) of **1–7** in DMSO-d_6 (δ in ppm, J in Hz)

No.	1	2	3	4	5	6	7
6	5.86, s	5.93, d (1.6)	5.90, d (1.6)	5.88, d (1.9)	5.76, s	6.17, s	6.12, s
8	5.78, s	5.86, d (1.6)	5.86, d (1.6)	5.86, d (1.9)	5.73, s		
2′	6.89, s	7.28, d (8.7)	6.90, d (1.6)	7.29, d (8.8)	6.89, d (2.0)	7.97, d (8.7)	7.82, d (2.0)
3′		6.79, d (8.7)		6.79, d (8.8)		6.84, d (8.7)	
5′	6.72, d (8.6)	6.79, d (8.7)	6.74, d (8.4)	6.79, d (8.8)	6.73, d (8.3)	6.84, d (8.7)	6.80, d (8.5)
6′	6.75, d (8.6)	7.28, d (8.7)	6.76, dd (8.4, 1.6)	7.29, d (8.8)	6.76, dd (8.3, 2.0)	7.97, d (8.7)	7.54, dd (8.5, 2.0)
6″			6.71, s	6.69, s	6.67, s		6.16, s
8″	7.01, s	7.00, s					
2‴	8.08, d (8.5)	7.72, d (1.9)	8.16, d (8.8)	7.88, d (2.2)	7.89, d (2.0)	7.97, d (8.7)	8.01, d (8.8)
3‴	6.94, d (8.5)		6.94, d (8.8)			6.84, d (8.7)	6.83, d (9.0)
5‴	6.94, d (8.5)	6.91, d (8.5)	6.94, d (8.8)	6.90, d (8.5)	6.90, d (8.6)	6.84, d (8.7)	6.83, d (9.0)
6‴	8.08, d (8.5)	7.58, dd (8.5, 1.9)	8.16, d (8.8)	7.64, dd (8.5, 2.2)	7.65, dd (8.6, 2.0)	7.97, d (8.7)	8.01, d (8.8)
8-CH_2-8″						4.22, s	4.24, s
5-OH						12.53, s	12.52, s
5″-OH							12.53, s

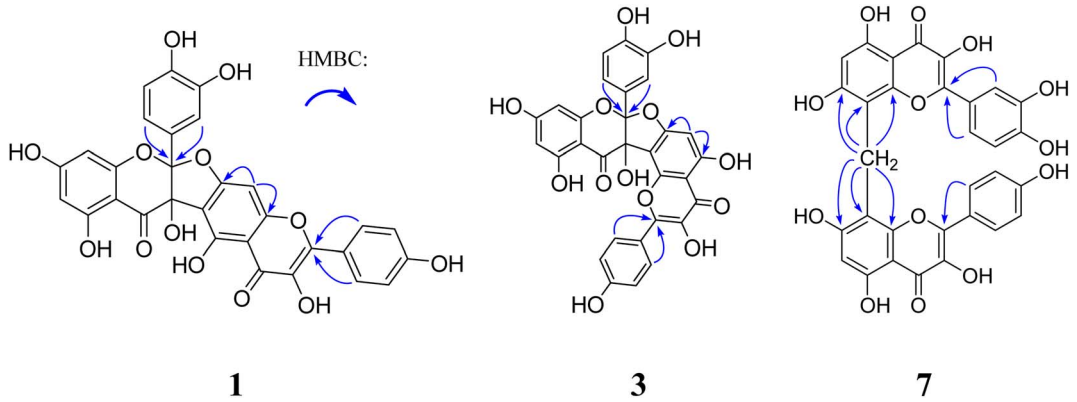

Fig. 2 Key HMBC correlations of compounds **1**, **3** and **7**.

on the positive HR-ESI-MS ion observed at *m*/*z* 587.0824 $[M + H]^+$ (Calcd 587.0826). Its ^{13}C and ^1H NMR spectra (Tables 1 and 2) were quite similar to those of **1**, except that quercetin and dihydrokaemferol subunit in **2** were observed instead of kaempferol and dihydroquercetin subunit respectively in **1**. Those were further supported by HMBC cross peak of the aromatic protons δ_H 7.72 (1H, d, $J = 1.9$ Hz, H-2‴) and 7.58 (1H, dd, $J = 8.5$, 1.9 Hz, H-6‴) with C-2″ (δ_C 148.0), of the aromatic proton δ_H 7.28 (2H, d, $J = 8.7$ Hz, H-2′, 6′) with C-2 (δ_C 117.8). The lack of optical activity and Cotton effect in the ECD spectrum indicated that **2** was a racemic mixture. Chiral HPLC resolution of **2** gave **2a** and **2b** in a ratio of approximately 1 : 1. Comparison between the experimental and calculated ECD spectra of two enantiomers allowed the absolute configurations of **2a** and **2b** to be established as (2*S*,3*S*) and (2*R*, 3*R*), respectively. Thus, compounds **2a** and **2b** were determined as (2*S*,3*S*)-3,5,7,4′-tetrahydroxyflavanone-(2-O-7″:3-6″)-3″,5″,3‴,4‴-tetrahydroxyflavone and (2*R*,3*R*)-3,5,7,4′-tetrahydroxyflavanone-(2-O-7′:3-6″)-3″,5″,3‴,4‴-tetrahydroxyflavone, and named as (+)-dysosmabiflavonoid B and (−)-dysosmabiflavonoid B, respectively.

Compounds **3** and **4** were obtained as yellow, amorphous powders. They possessed the same molecular formula $C_{30}H_{18}O_{13}$ as that of **1** and **2**, as revealed from their HR-ESI-MS analyses (*m*/*z* 587.0808 $[M + H]^+$ in **3**; *m*/*z* 587.0800 $[M + H]^+$ in **4**). Their ^{13}C and ^1H NMR data (Tables 1 and 2) were quite similar to those of **1** and **2**, except that the chemical shift changes of an aromatic carbon and an aromatic proton [from δ_C 94.8 (C-6″), δ_H 6.71 (1H, s, H-6″) in **3** to δ_C 91.1 (C-8″), δ_H 7.01 (1H, s, H-8″) in **1**, from δ_C 94.7 (C-6″), δ_H 6.69 (1H, s, H-8″) in **4** to δ_C 91.1 (C-8″), δ_H 7.00 (1H, s, H-8″) in **2**, indicating the subunits of kaempferol in **3** and quercetin in **4** were substituted at C-7 and C-8. Those were also supported by chemical shift change from δ_C 94.8 (C-6″), 164.9 (C-7″), and 106.3 (C-8″) in **3** to δ_C 98.2 (C-6), 163.9 (C-7), and 93.5 (C-8) in kaempferol [17], and from δ_C 94.7 (C-6″), 164.8 (C-7″), and 106.1 (C-8″) in **4** to δ_C 98.6 (C-6), 164.3 (C-7), and 93.8 (C-8) in quercetin.[19] Compounds **3** and **4** were also racemic mixtures, and separated into **3a** and **3b**, and **4a** and **4b**, respectively. The absolute configurations of **3a**, **3b**, **4a**, **4b** were determined as (2*S*, 3*S*), (2*R*, 3*R*), (2S, 3S), (2*R*, 3*R*) by comparison of their experimental and calculated ECD spectra. Thus, compounds **3a**, **3b**, **4a** and **4b** were deduced as (2*S*,3*S*)-3,5,7,3′,4′-pentahydroxyflavanone-(2-O-7″:3-8″)-3″,5″,4‴-trihydroxyflavone, (2*R*,3*R*)-3,5,7,3′,4′-pentahydroxyflavanone-(2-O-7′:3 → 8″)-3″,5″,4‴-trihydroxyflavone, (2*S*,3*S*)-3,5,7,4′-tetrahydroxyflavanone-(2-O-7″:3-8″)-3″,5″,3,4‴-tetrahydroxyflavone, and (2*R*,3*R*)-3,5,7,4′-tetrahydroxyflavanone-(2-O-7″:3-8″)-3″,5″,3‴,4‴-tetrahydroxyflavone, and named as (−)-dysosmabiflavonoid C, (+)-dysosmabiflavonoid C, (−)-dysosmabiflavonoid D, and (+)-dysosmabiflavonoid D, respectively.

Compound **5** was obtained as a yellow amorphous powder. Its ^1H and ^{13}C NMR spectra data (Tables 1 and 2) were quite analogous to those of **4**, except that 1,3,4-trisubstituted benzene ring δ_H 6.89 (1H, d, $J = 2.0$ Hz), 6.73 (1H, d, $J = 8.3$ Hz), 6.76 (1H, dd, $J = 8.3$, 2.0 Hz) was observed in **5** instead of 1,4-disubstituted benzene ring in **4**. This was further supported by their HR-ESI-MS, which gave an $[M + H]^+$ quasi-molecular ion peak *m*/*z* 603.0752 (Calcd 603.0775) in **5**, being 16 mass-units more than that of **4**. The dihydroquercetin subunit was identified as by the HMBC cross peak of the aromatic protons δ_H 6.89 (1H, d, $J =$ 2.0 Hz, H-2′) and 6.76 (1H, dd, $J = 8.3$, 2.0 Hz, H-6′) with C-2 (δ_C 117.8), one 1,2,3,5-tetra-substituted benzene ring δ_H 5.76 (1H, s), 5.73 (1H, s), and two oxygenated aliphatic quaternary carbons δ_C 117.8, 79.9. The apparent lack of a Cotton effect in ECD spectrum indicated that **5** was a racemic mixture. Compounds **5a** and **5b** were obtained as a pair of enantiomers by chiral-phase HPLC isolation of **5**. The absolute configurations of **5a** and **5b** were determined as (2*S*, 3*S*) and (2*R*, 3*R*) by comparison of calculated ECD and experimental data. Thus, compound **5** was deduced as (2*S*,3*S*)-3,5,7,3′,4′-pentahydroxyflavanone-(2-O-7″:3-8″)-3″,5″,3‴,4‴-tetrahydroxyflavone and (2*R*,3*R*)-3,5,7,3′,4′-pentahydroxyflavanone-(2-O-7″:3-8″)-3″,5′′,3‴,4‴-tetrahydroxyflavone, (−)-dysosmabiflavonoid E, and (+)-dysosmabiflavonoid E, respectively.

Compound **6** was obtained as a yellow amorphous powder and possessed a molecular formula $C_{31}H_{20}O_{12}$ with twenty-two degrees of unsaturation, as revealed from its HR-ESI-MS analysis (*m*/*z* 585.1023 $[M + H]^+$, calcd for $C_{31}H_{21}O_{12}$, 585.1033). The IR spectrum displayed the conjugated carbonyl group (1647 cm^{-1}), hydroxy groups (3361 cm^{-1}), and aromatic ring (1510 cm^{-1}). The UV spectrum exhibited absorption maxima

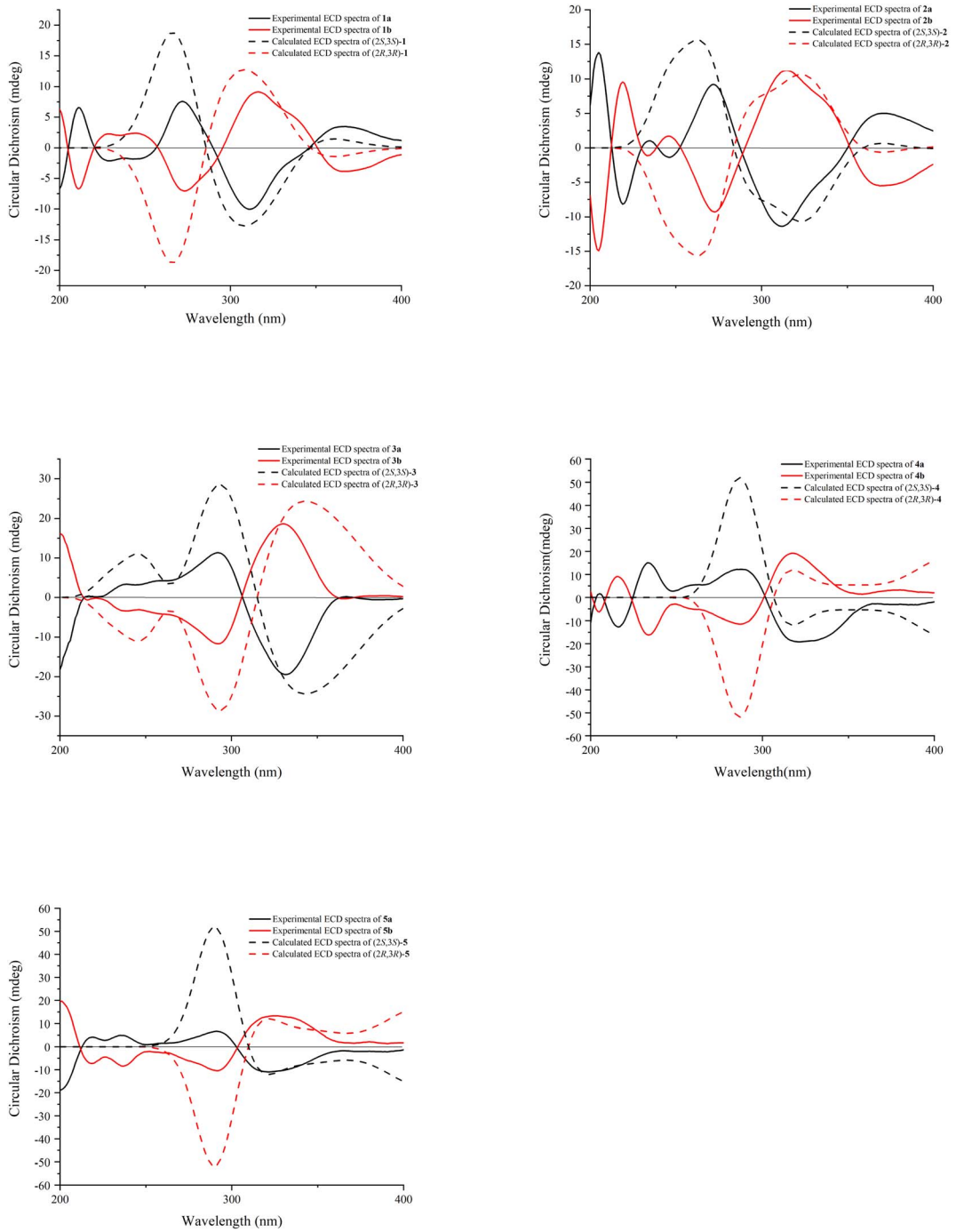

Fig. 3 Experimental and calculated ECD spectra of compounds **1a–5a** and **1b–5b**.

characteristic for flavonol at 271 and 369 nm. The ^{1}H NMR spectrum showed two sets of aromatic systems including one para-disubstituted benzene ring δ_H 7.97 (2H, d, J = 8.7 Hz), 6.84 (2H, d, J = 8.7 Hz), and one penta-substituted benzene ring δ_H 6.17 (1H, s), and one isolated aliphatic proton δ_H 4.22 (1H, s). The ^{13}C NMR and HSQC spectrum revealed one aliphatic carbon δ_C 16.4 and one flavonol skeleton including one carbonyl group δ 176.2, two benzene rings, two oxygen-bearing olefinic carbons δ_C 146.9, 135.4. Its ^{1}H NMR spectrum was almost similar to that of kaempferol, except that an extra proton signal at δ_H 4.22 (1H, s) was observed in **6** instead of one aromatic proton signal at δ_H 6.48 (1H, br s) in kaempferol.[17] In combination with the molecular formula $C_{31}H_{20}O_{12}$, two symmetrical kaempferol moieties were linked at C-8 and C-8′ by one methylene group. This was also supported by the HMBC correlations of the methylene group δ_H 4.22 (2H, s) with C-7 and C-7″ (δ_C 162.1), C-8 and C-8″ (δ_C 104.6), and C-9 and C-9″ (δ_C 153.8). Thus, compound **6** was deduced as 3,5,7,4′,3″,5″,7″,4‴-

octahydroxyl-[8-CH_2-8′]-biflavone, and named dysosmabiflavonoid F.

Compound **7** was obtained as a yellow amorphous powder. Its ^{1}H and ^{13}C NMR (Tables 1 and 2) were quite analogous to those of **6**, except that one 1,3,4-trisubstituted benzene ring δ_H 7.82 (1H, d, $J = 2.0$ Hz), 6.80 (1H, d, $J = 8.5$ Hz), 7.54 (1H, dd, $J =$ 8.5 2.0 Hz) was observed in **7** instead of 1,4-disubstituted benzene ring in **6**. This was further supported by their HR-ESI-MS, which gave an $[M + Na]^+$ quasi-molecular ion peak m/z 623.0799 (Calcd 623.0802) in **7**, being 16 mass-units more than that of **6**. The quercetin subunit was identified as by the HMBC cross peak of the aromatic protons δ_H 7.82 (1H, d, $J = 2.0$ Hz, H-2′) and 7.54 (1H, dd, $J = 8.5$, 2.0 Hz, H-6′) with C-2 (δ 146.7), one 1,2,3,4,5-tetra-substituted benzene ring δ_H 6.12 (1H, s), and two oxygenated olefinic carbons δ_C 146.7, 135.4. Thus, compound **7** was 3,5,7,3′,4′,3″,5″,7″,4‴-nonahydroxyl-[8-CH_2-8′]-biflavone, and named dysosmabiflavonoid G.

By comparing their physical and spectroscopic data with literature values, the known metabolites were identified as kaempferol (**8**),[17] quercetin (**9**),[19] dihydrokaempferol (**10**),[20] dihydroquercetin (**11**).[20]

All the isolates (**1–11**) were evaluated for their acetylcholinesterase inhibitory activity, using a modified spectrophotometric method.[21] Tacrine was utilized as the positive control. The results are listed in Table 3 as IC_{50} values. Based on the IC_{50} values, all racemates **1–5** exhibited satisfactory AChE inhibitory activity in the range of micromolar concentrations (IC_{50} values 2.72–6.74 μM), and more potent inhibitory activity than their corresponding levorotatory or dextrorotatory enantiomers. Among all of biosynthetically related precursors (**8–11**), only quercetin (**9**) are more active than racemates **2–5**. The combination between quercetin and dihydrokaempferol or between quercetin and dihydroquercetin by a furan ring reduced the inhibitory activity, for example, compared **2**, **4** and **5** to **9**. However, this phenomenon is inverse the combination between kaempferol and dihydrokaempferol or between kaempferol and dihydroquercetin, for example, compared **1** and **3** to **8**. Hydrogenation (**10** and **11**) at C-2 and C-3 drastically reduced the inhibitory activity of the flavonol derivatives (**8** and **9**). The hydroxy group at C-3′ is important, as 3′,4′-dihydroxy derivative **9** showed more potent activity than its corresponding 4′-hydroxy analogue **8**. The methylene linkage bridge between flavonol skeletons plays a very important role in maintaining inhibitory activity for this series of biflavonoids, for example, compared **8** and **9** to **7**, and **8** to **6**. In terms of the structure, racemates **1–5** are different completely from general biflavonoids. Moreover, due to the similarity in AChE inhibitory activity, they can be used as a template for the development of new drugs against neurodegenerative diseases.

Racemates **1–5** and their corresponding levorotatory and dextrorotatory enantiomers were measured for the potential to impede the generation of NO in lipopolysaccharide-stimulated RAW264.7 cells,[22] and mushroom tyrosinase inhibitory effect.[23] Unfortunately, they were inactive ($IC_{50} > 50$ μM) against the inhibition of NO production. Only racemates **1** and **2** were found to display potent mushroom tyrosinase inhibitory activity with IC_{50} values of 28.27 μM and 39.75 μM (the positive control, kojic acid, 32.59 μM), respectively, whereas racemates **3–5** displayed no inhibitory effect against tyrosinase activity. The variation in inhibitory activity between them indicates the linkage bridges of C-2-O-C-7″:C-3-C-6″ were structurally required for anti-tyrosinase activity. Racemate **1**, as the most potent tyrosinase inhibitor, has the therapeutic potential for skin hyperpigmentation and depigmentation in cosmetics.

Table 3 AChE inhibitory activities of all isolated compounds

No.	IC_{50} (μM)	No.	IC_{50} (μM)
1	2.72 ± 0.25	**5**	6.74 ± 0.04
1a	32.95 ± 2.90	**6**	1.42 ± 0.14
1b	6.25 ± 0.57	**7**	0.73 ± 0.07
2	4.55 ± 0.36	**8**	17.90 ± 0.18
2a	4.97 ± 1.80	**9**	3.96 ± 0.27
3	6.39 ± 0.48	**11**	43.95 ± 2.43
3a	10.65 ± 1.43	**2b**, **4a**, **4b**, **5a**, **5b**, **10**	>50
3b	9.89 ± 0.71	Tacrine	0.21 ± 0.01
4	6.33 ± 0.45		

Conclusions

So far, more than 600 natural biflavonoids have been found, and the vast majority of them are isolated from the plants of families Clusiaceae, Thymelaeaceae, Ochnaceae, and Selaginellaceae, *etc.*[24] Only eleven biflavonoids have been obtained from plants of the genus *Dysosma*.[13–16] Our phytochemical investigations on *D. versipellis* resulted in the isolation of five pairs of new biflavonoid enantiomers, (±)-dysosmabiflavonoids A–E (**1–5**), two new biflavonoids, dysosmabiflavonoids F–G (**6–7**), along with four biosynthetically related precursors (**8–11**). Racemates **1–2** represent the first report of natural C-2-O-C-7′:C3-C6″ biflavonoids. Based upon the IC_{50} values, compound **7** was the most potent AChE inhibitor among all isolated compounds. Further studies on compound **7** are necessary to action mechanism and *in vivo* efficacy in neurodegenerative diseases. Above all, the present investigation will broaden the application field of *D. versipellis*.

Experimental method

General experimental procedures

Optical rotations and ECD spectra were measured by a Rudolph AP-IV polarimeter and an Applied Photophysics Chirascanq CD spectropolarimeter, respectively. UV and IR spectra were acquired using a ThermoEVO 300 spectrometer and a Thermo-Nicolet IS 10 spectrometer, respectively. NMR and mass spectra were recorded on a Bruker Avance III 500 spectrometer and a Bruker maXisHD mass spectrometer, respectively. Preparative HPLC separations were performed on a SEP system (Beijing Sepuruisi scientific Co., Ltd, China) equipped with a variable-wavelength UV detector, using a YMC-Pack ODS-A column (250 × 20 mm, 5 μm) and a Daicel chiral PAK AD-H column (250 × 10 mm, 5 μm). Sephadex LH-20 (40–70 μm), and silica gel (160–200 mesh) were acquired from Amersham Pharmacia Biotech AB, Uppsala, Sweden, and Marine Chemical Industry,

Qingdao, China, respectively. Chemical reagents for isolation were of analytical grade and purchased from Tianjin Siyou Co., Ltd, China. Biological reagents were from Sigma Company.

Plant material

The roots and rhizomes of *D. versipellis* were collected in Qingzhen, Guizhou Province, China, in July 2019, and identified by Prof. Cheng-Ming Dong at School of Pharmacy, Henan University of Chinese Medicine, where a voucher specimen (DV 20190706) was deposited.

Extraction and isolation

The powder of air-dried roots and rhizomes of *D. versipellis* (40 kg) were refluxed with 95% EtOH (v/v 120 L × 3, 1.5 h each) and 50% EtOH (v/v 120 L × 1, 1.5 h each) at 95 °C, respectively. The filtrate was concentrated under reduced pressure to yield a dark brown residue (5.4 kg). The residue was adsorbed by silicious earth and fractioned by CH_2Cl_2, EtOAc, and MeOH. The MeOH extract (3.4 kg) was separated into nine fractions M1–M9 by silica gel column chromatography (CC) with a gradient of CH_2Cl_2–MeOH (v/v 100 : 0, 100 : 1, 100 : 3, 100 : 5, 100 : 7, 100 : 10, 100 : 30, 100 : 50, 0 : 100) based on TLC monitoring results. Fraction M5 (110.0 g) was subjected to sephadex LH-20 CC eluted by methanol to yield subfractions M5-1–M5-8. Subfraction M5-8 (42.5 g) was submitted to silica gel CC eluted by PE–acetone (100 : 10, 100 : 20, 100 : 30, 100 : 40, 100 : 50, 100 : 70, 1 : 1, 1 : 2, 1 : 3) to afford nine subfractions (M5-8-1–M5-8-9). Subfraction M5-8-4 (0.5 g) was isolated by preparative HPLC ($MeOH : H_2O$, 60 : 40) at a flow rate of 3 mL min^{-1} to give compound **8** (t_R 40.5 min, 10.0 mg) and **6** (t_R 47.2 min, 6.0 mg). Subfraction M5-8-5 (1.07 g) was separated by preparative HPLC ($MeOH : H_2O$, 55 : 45) at a flow rate of 3 mL min^{-1} to afford subfractions [M5-8-5-1, (±) **2**, t_R 37.4 min, 8.5 mg], (M5-8-5-2, t_R 46.0 min, 78.2 mg), (M5-8-5-3, t_R 72.2 min, 90.1 mg), [M5-8-5-4, (±) **3**, t_R 77.0 min, 12.9 mg]. Subfraction M5-8-5-1 was isolated by preparative chiral HPLC (cyclohexane : isopropanol, 60 : 40) at a flow rate of 2 mL min^{-1} to give **2a** (t_R 7.9 min, 3.6 mg) and **2b** (t_R 18.0 min, 3.6 mg). Subfraction M5-8-5-2 was chromatographed by preparative HPLC ($CH_3CN : H_2O$, 45 : 55) at a flow rate of 3 mL min^{-1} to give subfractions [M5-8-5-2-1, (±) **5**, t_R 25.7 min, 6 mg], [M5-8-5-2-2, (±) **1**, t_R 29.1 min, 9.4 mg] and compound **11** (t_R 20.6 min, 10.9 mg). Subfraction M5-8-5-2-1 was isolated by preparative chiral HPLC (cyclohexane : isopropanol, 81 : 19) at a flow rate of 2 mL min^{-1} to give **5a** (t_R 31.8 min, 2.4 mg) and **5b** (t_R 43.8 min, 2.4 mg). Subfraction M5-8-5-2-2 was subjected to preparative chiral HPLC (cyclohexane : isopropanol, 60 : 40) at a flow rate of 2 mL min^{-1} to give **1a** (t_R 7.8 min, 4.2 mg) and **1b** (t_R 21.4 min, 4.2 mg). Subfraction M5-8-5-3 was isolated by preparative HPLC ($CH_3CN : H_2O$, 43 : 57) at a flow rate of 3 mL min^{-1} to give subfractions [M5-8-5-3-1, (±) **4**, t_R 26.9 min, 5.5 mg] and **10** (t_R 22.5 min, 5.5 mg). Subfraction M5-8-5-3-1 was isolated by preparative chiral HPLC (cyclohexane: isopropanol, 81 : 19) at a flow rate of 2 mL min^{-1} to give **4a** (t_R 20.8 min, 2.5 mg) and **4b** (t_R 30.2 min, 2.5 mg). Subfraction M5-8-5-4 was submitted to preparative chiral HPLC (cyclohexane : isopropanol, 70 : 30) at a flow rate of 2 mL min^{-1} to give **3a** (t_R 9.7 min, 5.0 mg) and **3b** (t_R 12.7 min, 5.0 mg). Fraction M6 (130.0 g) was subjected to sephadex LH-20 CC eluted by methanol to yield subfractions M6-1, M6-2 and **11** (5 mg). The subfraction M6-2 (60.5 g) was applied to silica gel CC with a CH_2Cl_2–MeOH (100 : 1, 100 : 3, 100 : 5, 100 : 7, 100 : 10, 100 : 30) gradient to give six subfractions (M6-2-1–M6-2-6). Further separation of M6-2-4 (1.69 g) using sephadex LH-20 CC eluted by MeOH resulted in six subfractions M6-2-4-1–M6-2-4-6. Subfractions M6-2-4-4 (0.59 g) was purified by preparative HPLC ($MeOH : H_2O$, 60 : 40) at a flow rate of 3 mL min^{-1} to afford compounds **7** (t_R 24.1 min, 3.0 mg) and **9** (t_R 20.4 min, 8.0 mg).

(±)-Dysosmabiflavonoid A (1). Yellow, amorphous powder; UV (MeOH) λ_{max} (log ε) 202 (4.33), 275 (3.58), 360 (3.52) nm; IR (iTR) ν_{max} 3374, 2958, 2928, 2853, 1726, 1635, 1607, 1512, 1465, 1374, 1284, 1179, 1123, 1075, 1022 cm^{-1}; HR-ESI-MS (positive): *m*/*z* 587.0806 $[M + H]^+$ (Calcd for $C_{30}H_{19}O_{13}$, 587.0826), *m*/*z* 609.0642 $[M + Na]^+$ (Calcd for $C_{30}H_{18}O_{13}Na$, 609.0645), *m*/*z* 625.0370 $[M + K]^+$ (Calcd for $C_{30}H_{18}O_{13}K$, 625.0384); NMR data (DMSO-d_6), see Tables 1 and 2

(+)-Dysosmabiflavonoid A (1a). Yellow, amorphous powder; $[\alpha]_D^{20}$ + 41.5 (*c* 0.07, MeOH); ECD (MeOH) λ_{max} ($\Delta\varepsilon$) 229 (−0.8), 243 (−0.7), 272 (+2.7), 311 (−3.6), 367 (+1.2) nm.

(−)-Dysosmabiflavonoid A (1b). Yellow, amorphous powder; $[\alpha]_D^{20}$ − 41.8 (*c* 0.08, MeOH); ECD (MeOH) λ_{max} ($\Delta\varepsilon$) 229 (+0.8), 243 (+0.9), 273 (−2.5), 316 (+3.2), 368 (−1.4) nm.

(±)-Dysosmabiflavonoid B (2). Yellow, amorphous powder; UV (MeOH) λ_{max} (log ε) 202 (4.54), 256 (3.92), 298 (3.85), 370 (3.84) nm; IR (iTR) ν_{max} 3374, 2958, 2920, 2850, 1727, 1636, 1519, 1465, 1368, 1282, 1169, 1123, 1075, 1023 cm^{-1}; HR-ESI-MS (positive): *m*/*z* 587.0824 $[M + H]^+$ (Calcd for $C_{30}H_{19}O_{13}$, 587.0826), *m*/*z* 609.0642 $[M + Na]^+$ (Calcd for $C_{30}H_{18}O_{13}Na$, 609.0645), *m*/*z* 625.0383 $[M + K]^+$ (Calcd for $C_{30}H_{18}O_{13}K$, 625.0384); NMR data (DMSO-d_6), see Tables 1 and 2.

(+)-Dysosmabiflavonoid B (2a). Yellow, amorphous powder; $[\alpha]_D^{20}$ + 39.0 (*c* 0.07, MeOH); ECD (MeOH) λ_{max} ($\Delta\varepsilon$) 219 (−2.9), 246 (−0.5), 272 (+3.3), 312 (−4.0), 370 (+1.8) nm.

(−)-Dysosmabiflavonoid B (2b). Yellow, amorphous powder; $[\alpha]_D^{20}$ − 42.0 (*c* 0.05, MeOH); ECD (MeOH) λ_{max} ($\Delta\varepsilon$) 219 (+3.4), 246 (+0.6), 273 (−3.3), 314 (+4.0), 369 (−2.0) nm.

(±)-Dysosmabiflavonoid C (3). Yellow, amorphous powder; UV (MeOH) λ_{max} (log ε) 203 (4.64), 271 (3.87), 299 (3.88), 367 (3.79) nm; IR (iTR) ν_{max} 3382, 2959, 2931, 2872, 1725, 1638, 1607, 1514, 1466, 1385, 1353, 1282, 1124, 1075, 1024 cm^{-1}; HR-ESI-MS (positive): *m*/*z* 587.0808 $[M + H]^+$ (Calcd for $C_{30}H_{19}O_{13}$, 587.0826), *m*/*z* 609.0639 $[M + Na]^+$ (Calcd for $C_{30}H_{18}O_{13}Na$, 609.0645), *m*/*z* 625.0375 $[M + K]^+$ (Calcd for $C_{30}H_{18}O_{13}K$, 625.0384); NMR data (DMSO-d_6), see Tables 1 and 2

(−)-Dysosmabiflavonoid C (3a). Yellow, amorphous powder; $[\alpha]_D^{20}$ − 63.9 (*c* 0.06, MeOH); ECD (MeOH) λ_{max} ($\Delta\varepsilon$) 235 (+2.1), 290 (+4.0), 327 (−6.9), 379 (−0.2) nm.

(+)-Dysosmabiflavonoid C (3b). Yellow, amorphous powder; $[\alpha]_D^{20}$ + 66.0 (*c* 0.05, MeOH); ECD (MeOH) λ_{max} ($\Delta\varepsilon$) 236 (−2.4), 291 (−5.0), 327 (+7.9), 379 (+0.3) nm.

(±)-Dysosmabiflavonoid D (4). Yellow, amorphous powder; UV (MeOH) λ_{max} (log ε) 202 (4.42), 257 (3.91), 299 (3.85), 379 (3.71) nm; IR (iTR) ν_{max} 3364, 2925, 2853, 1738, 1640, 1614,

1519, 1466, 1326, 1258, 1172, 1035 cm^{-1}; HR-ESI-MS (positive): *m/z* 587.0800 $[M + H]^+$ (Calcd for $C_{30}H_{19}O_{13}$, 587.0826), *m/z* 609.0636 $[M + Na]^+$ (Calcd for $C_{30}H_{18}O_{13}Na$, 609.0645), *m/z* 625.0371 $[M + K]^+$ (Calcd for $C_{30}H_{18}O_{13}K$, 625.0384); NMR data (DMSO-d_6), see Tables 1 and 2.

(−)-Dysosmabiflavonoid D (4a). Yellow, amorphous powder; $[\alpha]_D^{20}$ − 64.4 (*c* 0.05, MeOH); ECD (MeOH) λ_{max} ($\Delta\varepsilon$) 233 (+1.5), 288 (+1.2), 322 (−1.9), 380 (−0.3) nm.

(+)-DysosmabiflavonoidD (4b). Yellow, amorphous powder; $[\alpha]_D^{20}$ + 64.8 (*c* 0.03, MeOH); ECD (MeOH) λ_{max} ($\Delta\varepsilon$) 234 (−1.9), 287 (−1.4), 317 (+2.3), 377 (+0.4) nm.

(±)-Dysosmabiflavonoid E (5). Yellow, amorphous powder; UV (MeOH) λ_{max} (log ε) 203 (4.41), 257 (3.82), 297 (3.78), 380 (3.63) nm; IR (iTR) ν_{max} 3377, 2924, 2853, 1739, 1638, 1608, 1463, 1305, 1265, 1173, 1124, 1027 cm^{-1}; HR-ESI-MS (positive): *m/z* 603.0752 $[M + H]^+$ (Calcd for $C_{30}H_{19}O_{14}$, 603.0775), *m/z* 625.0593 $[M + Na]^+$ (Calcd for $C_{30}H_{18}O_{14}Na$, 609.0594), *m/z* 641.0313 $[M + K]^+$ (Calcd for $C_{30}H_{18}O_{14}K$, 641.0334); NMR data (DMSO-d_6), see Tables 1 and 2.

(−)-Dysosmabiflavonoid E (5a). Yellow, amorphous powder; $[\alpha]_D^{20}$ − 50.4 (*c* 0.05, MeOH); ECD (MeOH) λ_{max} ($\Delta\varepsilon$) 219 (+0.7), 235 (+0.8), 291 (+1.1), 321 (−1.8), 380 (−0.2) nm.

(+)-Dysosmabiflavonoid E (5b). Yellow, amorphous powder; $[\alpha]_D^{20}$ + 51.0 (*c* 0.04, MeOH); ECD (MeOH) λ_{max} ($\Delta\varepsilon$) 220 (−0.6), 237 (−0.7), 292 (−0.9), 326 (+1.2), 382 (+0.2) nm.

Dysosmabiflavonoid F (6). Yellow, amorphous powder; UV (MeOH) λ_{max} (log ε) 202 (4.89), 271 (4.69), 317 (4.46), 369 (4.51) nm; IR (iTR)ν_{max} 3361, 1647, 1563, 1510, 1379, 1266, 1188, 1159, 1022 cm^{-1}; HR-ESI-MS (positive): *m/z* 585.1023 $[M + H]^+$ (Calcd for $C_{31}H_{21}O_{12}$, 585.1033); NMR data (DMSO-d_6), see Tables 1 and 2.

Dysosmabiflavonoid G (7). Yellow, amorphous powder; UV (MeOH) λ_{max} (log ε) 202 (5.05), 270 (4.80), 328 (4.56), 372 (4.70) nm; IR (iTR)ν_{max} 3247, 1650, 1604, 1559, 1512, 1424, 1372, 1316, 1259, 1159, 1114 cm^{-1}; HR-ESI-MS (positive): *m/z* 623.0799 $[M + Na]^+$ (Calcd for $C_{31}H_{20}O_{13}Na$, 623.0802); NMR data (DMSO-d_6), see Tables 1 and 2.

AChE inhibitory assay *in vitro*

The AChE inhibitory activity was measured by a classical spectrophotometric method with minor modifications.[21] A 200 μL volume reaction system containing phosphate buffer (pH 8.0), tested compounds at different concentrations, and AChE (0.02 U mL^{-1}), was incubated for 20 min at 37 °C. Then, the reaction was initiated by the addition of 40 μL of solution containing DTNB (0.625 mM) and acetylthiocholine iodide (0.625 mM) for AChE inhibitory activity assay, respectively. The hydrolysis of acetylthiocholine was monitored at 405 nm every 30 seconds for one hour. All the reactions were performed in triplicate. The IC_{50} value of each compound was calculated by the Reed-Muench's method.

Assay for LPS-induced NO production

Test protocols were carried out as previously described.[22] RAW 264.7 macrophages cells (2×10^5 cells per well) were precultured in 96-well microplates for 24 h. The tested compounds (50 μM) and L-NMMA with 1 μg mL^{-1} LPS were added and incubated at 37 °C for another 18 h. Nitric oxide production was determined by the Griess Reagent System. L-N^G-monomethyl arginine (L-NMMA) was used as a positive control.

Assay for tyrosinase inhibitory activity

Tyrosinase inhibitory activity was measured using an established assay protocol, with slight modification.[23] The tested compound was dissolved phosphate buffer solution containing 0.2% DMSO. The 60 μL of phosphate buffer (20 mM, pH 6.8) and 50 μL of the tested compounds at different concentrations, and 50 μL of mushroom tyrosinase solution (20 μg mL^{-1}) were placed into each well of a 96-well cell culture plate. After incubation for 10 min at 25 °C, 40 μL of L-dopa (2.0 mM) was added to the reaction system. The reaction mixture was incubated for another 5 min, and the absorbance was measured at 490 nm. Kojic acid was used as standard agent. The IC_{50} value of each compound was calculated as the concentration of the sample when the residual enzyme activity is 50%.

ECD computational method

All the quantum chemical ECDs were calculated by the literature method.[25] Conformational searches of compounds **1a–5a** and **1b–5b** were investigated by Spartan software using the MMFF94S force field, which gave four stable conformers, respectively. Then, those selected conformers were further optimized by density functional theory method at the B3LYP/6-31G* level. The ECD of these optimized conformers were calculated by the TDDFT method at the B3LYP/6-31+G* level with a CPCM model in MeOH solvent.

Author contributions

R. J. Han, H. Y. Bai and H. J. Wang performed the experiments, data analysis, and experimental planning. M. Li, Y. Y. Si, J. M. Wang, J. H. Gong and H. Chen screened the biological activities. The project was conceived and supervised by Y. J. Sun and W. S. Feng. The manuscript was written by Y. J. Sun. All authors reviewed the manuscript.

Conflicts of interest

There are no conflicts to declare.

Acknowledgements

This work was supported by Basic Science Foundation of Henan University of Chinese Medicine (No. 2014KYYWF-QN26), Science and Technology Innovation Talent Support Scheme of Henan University of Chinese Medicine (No. 2016XCXRC01), Scientific and Technological Key Project in Henan Province (No. 192102310438), and Research Project on Chinese Medicine Science in Henan Province (No. 20-21ZY1039).

Notes and references

1 S. H. Lu, J. W. Wu, H. L. Liu, J. H. Zhao, K. T. Liu, C. K. Chuang, H. Y. Lin, W. B. Tsai and Y. Ho, *J. Biomed. Sci.*, 2011, **18**, 8.
2 M. Rosini, V. Andrisano, M. Bartolini, M. L. Bolognesi, P. Hreli, A. Minarini, A. Tarozzi and C. Melchiorre, *J. Med. Chem.*, 2005, **48**, 360–363.
3 M. Przybylowska, K. Dzierzbicka, S. Kowalski, K. Chmielewska and I. Inkielewicz-Stepniak, *Curr. Neuropharmacol.*, 2021, **19**, 1323–1344.
4 B. C. Guan, C. X. Fu, Y. X. Qiu, S. L. Zhou and H. P. Comes, *Am. J. Bot.*, 2010, **97**, 111–122.
5 C. X. Liu, C. N. Zhang, T. He, L. Sun, Q. Wang, S. Han, W. X. Wang, J. Kong, F. L. Yuan and J. M. Huang, *Ecotoxicol. Environ. Saf.*, 2020, **190**, 110073.
6 X. Q. Xu, X. H. Gao, L. H. Jin, P. S. Bhadury, K. Yuan, D. Y. Hu, B. A. Song and S. Yang, *Cell Div.*, 2011, **6**, 14.
7 L. Man, Y. Liu, S. Ananda, Z. Luo and L. Liu, *J. Med. Plants Res.*, 2010, **4**, 717–721.
8 N. W. Lu, Q. An, N. Li and Y. M. Dong, *J. Chromatogr. Sci.*, 2014, **52**, 514–519.
9 Y. C. Shi, H. P. Yuan, R. Zou and B. B. Liu, *Mitochondrial DNA*, 2019, **4**, 4218–4219.
10 H. L. Fan, J. B. Xuan, K. X. Zhang and J. L. Jiang, *Anal. Methods*, 2018, **10**, 371–380.
11 B. He, Y. Chen, H. Zhang, C. Y. Xia, Q. Zhang and W. Li, *Hortic. Environ. Biotechnol.*, 2018, **59**, 519–528.
12 X. M. Tan, Y. Q. Zhou, X. L. Zhou, X. H. Xia, Y. Wei, L. L. He, H. Z. Tang and L. Y. Yu, *Sci. Rep.*, 2018, **8**, 5929.
13 R. D. Chen, R. G. Duan, Y. N. Wei, J. H. Zou, J. W. Li, X. Y. Liu, H. Y. Wang, Y. Guo, Q. H. Li and J. G. Dai, *Fitoterapia*, 2015, **107**, 77–84.
14 Z. Yang, Y. Q. Wu, H. Zhou, X. J. Cao, X. H. Jiang, K. W. Wang and S. H. Wu, *RSC Adv.*, 2015, **5**, 77553–77564.
15 Z. Yang, Y. Q. Wu and S. H. Wu, *J. Chromatogr. A*, 2016, **1431**, 184–196.
16 Z. Yang, P. P. Guo, R. Han and J. M. Gao, *J. Sep. Sci.*, 2018, **41**, 3631–3643.
17 D. D. Zheng, J. Y. Ruan, Y. Zhang, J. J. Yan, T. Wang and Y. Zhang, *Chin. J. Med. Chem.*, 2020, **30**, 542–548.
18 K. M. Canuto, L. K. A. M. Leal, A. A. Lopes, C. M. Coleman, D. Ferreira and E. R. Silveira, *J. Braz. Chem. Soc.*, 2014, **25**, 639–647.
19 M. Q. An, L. R. Li, C. R. Li, S. Y. Zhong, H. Y. Jiang, L. P. Wu and J. Huang, *West China J. Pharm. Sci.*, 2019, **34**, 577–582.
20 L. Chen, J. F. Xu and L. C. Sun, *Chin. Med. Mater.*, 2016, **39**, 90–93.
21 C. L. Yang, H. M. Wu, C. L. Liu, X. Zhang, Z. K. Guo, Y. Chen, F. Liu, Y. Liang, R. H. Jiao, R. X. Tan and H. M. Ge, *J. Nat. Prod.*, 2019, **82**, 792–797.
22 Z. Z. Zhao, Q. L. Zhao, W. S. Feng, H. R. He, M. Li, G. M. Xue, H. P. Chen and J. K. Liu, *RSC Adv.*, 2021, **11**, 18693–18701.
23 Y. J. Zhai, G. M. Huo, Q. Zhang, D. Li, D. C. Wang, J. Z. Qi, W. B. Han and J. M. Gao, *J. Nat. Prod.*, 2020, **83**, 1592–1597.
24 X. Q. He, F. Yang and X. A. Huang, *Molecules*, 2021, **26**, 6088.
25 Y. Y. Si, W. W. Wang, Q. M. Feng, Z. Z. Zhao, G. M. Xue, Y. J. Sun, W. S. Feng, J. I. Yong and X. S. Wang, *RSC Adv.*, 2021, **11**, 27085–27091.